ATTITUDE MOTION OF ORBITAL DEBRIS: DATA FROM GROUND-BASED RADAR AND ADRAS-J OBSERVATIONS

Hiroyuki Okamoto[*], Yuki Ikeda[†], Shinji Mitani[‡], Ryo Nakamura[‡], Toru Yamamoto[‡], Lars Fuhrmann[§], Frank Schlichthaber[**], and Taro Kashiwayanagi[††]

The attitude motion of orbital debris is a critical factor in the execution of Active Debris Removal (ADR) operations. Numerical simulations were conducted to examine the motion of a spent rocket upper stage in low Earth orbit (LEO). The findings demonstrated that, even with an initial rotation velocity, eddy current torque gradually decelerates the rotation, while gravity-gradient torque stabilizes the object, rendering it nearly stationary relative to the Local Vertical Local Horizontal (LVLH) frame. Ground-based observations of the rocket upper stage, performed by the Fraunhofer Institute using the TIRA radar, corroborated the numerical simulation results, confirming the stationary attitude of the upper stage within the LVLH frame. JAXA initiated the Commercial Removal of Debris Demonstration (CRD2) project to validate the feasibility of ADR technologies. Phase I of the CRD2 initiative emphasizes the rendezvous and imaging of uncooperative debris, targeting a spent H-IIA upper stage. Within this framework, the ADRAS-J demonstration satellite, developed and operated by Astroscale, successfully approached the H-IIA upper stage - remaining in LEO for over 15 years - to a proximity of 50 meters. Observations conducted by ADRAS-J confirmed that the upper stage maintains an attitude nearly stationary within the LVLH frame, as predicted by the numerical simulations.

INTRODUCTION

The increasing density of space debris in key orbital regions poses a significant threat to operational satellites, with potential collisions generating further debris and exacerbating the problem, jeopardizing the long-term sustainability of space activities. Active Debris Removal (ADR), which entails the removal of large space debris from congested orbits, is widely regarded as essential for maintaining a sustainable orbital environment.[1] Although several advanced ADR technologies

[*] Associate Senior Researcher, Research and Development Directorate, Japan Aerospace Exploration Agency (JAXA), 2-1-1 Sengen, Tsukuba, Ibaraki, 305-8505, Japan, +81-70-3370-7400, okamoto.hiroyuki@jaxa.jp
[†] Researcher, Research and Development Directorate, Japan Aerospace Exploration Agency (JAXA), 2-1-1 Sengen, Tsukuba, Ibaraki, 305-8505, Japan,
[‡] Senior Researcher, Research and Development Directorate, Japan Aerospace Exploration Agency (JAXA), 2-1-1 Sengen, Tsukuba, Ibaraki, 305-8505, Japan.
[§] Senior Scientist, Radar for Space Situational Awareness (RWL) section, Fraunhofer Institute for High Frequency Physics and Radar Techniques FHR, Fraunhoferstraße 20, 53343 Wachtberg, Germany.
[**] Scientist, Radar for Space Situational Awareness (RWL) section, Fraunhofer Institute for High Frequency Physics and Radar Techniques FHR, Fraunhoferstraße 20, 53343 Wachtberg, Germany.
[††] Manager, Computer Vision & Robotics Software, Astroscale Japan Inc., 4-17-1 Kinshi, Sumida, Tokyo, 130-0013, Japan.

have been proposed, none have yet been publicly demonstrated in orbit.[2] In an ADR operation, the attitude dynamics of the client debris is of critical importance, particularly concerning the rendezvous system, capture mechanism, and post-capture attitude control system. If the client debris exhibits high angular velocity, the ADR spacecraft must accommodate the debris' rotation; however, establishing precise design criteria remains challenging in the absence of specific information about the state of the client debris' attitude motion.

Ground-based observations, such as those conducted with optical telescopes or imaging radar, offer valuable insights into the characteristics of both rotating and stationary objects. Some studies have focused on determining the attitude motion of debris via light-curves produced from photometric measurements, which have proven to be useful for categorizing debris into fast-rotating or slowly tumbling objects.[3, 4] However, the fluctuations in the light curve are influenced not only by the debris' motion but also by scintillation effects caused by the Earth's atmosphere. Furthermore, it is challenging to derive the attitude state information if its motion is very slow. In addition, some cases indicate a repeatedly changing period of the attitude motion which cannot be easily explained,[5, 6] and difficult to explain or understand this behavior.

JAXA is developing a new ADR technology that includes rendezvousing with uncooperative client debris, including subsequent capture and deorbiting operations using a highly efficient propulsion system integrated into the ADR spacecraft. JAXA has launched the Commercial Removal of Debris Demonstration (CRD2) project* to assess the overall technological feasibility of ADR systems.[7, 8] The CRD2 project is divided into two phases: Phase 1 is dedicated to the rendezvous and imaging of an uncooperative client, while Phase 2 involves the rendezvous, capture, and deorbiting of the large debris. The target space debris for CRD2 has been selected from Japan’s rocket upper stage, and H-IIA upper stage which launched GOSAT in 2009 has been selected. At the selection time few attitude motion expectations were available, i.e. numerical simulation results.

The Fraunhofer Institute for High Frequency Physics and Radar Techniques (FHR) operates the Tracking and Imaging Radar (TIRA),[9, 10] which allows to utilize inverse synthetic aperture radar (ISAR) techniques for generating ground-based radar images and image sequences to estimate the attitude motion of space objects.[11] JAXA enlisted FHR to observe the client debris for CRD2 Phase 1, and TIRA conducted observations over a period of three years.

The CRD2 Phase 1 spacecraft, named ADRAS-J, was developed and operated by Astroscale Japan.[12] ADRAS-J approached the spent H-IIA upper stage and captured still images of this upper stage using an onboard optical camera. By analyzing multiple images, the attitude motion of the debris was estimated.

This paper presents a unique contribution by combining and validating numerical simulation, ground-based radar observations from TIRA, and close-proximity on-orbit observations from ADRAS-J to characterize the attitude motion of a H-IIA upper stage.

NUMERICAL SIMULATION

To analyze the long-term behavior of the H-IIA upper stage's attitude motion, numerical simulations were conducted using simplified model assumptions. When a conductive object rotates within a magnetic field, an eddy current is induced according to Lenz's law which generates a loop current. These eddy currents apply a torque to the rotating object, which can decelerate its rotational velocity or induce precession of its spin axis. Given the fact that most spent rocket upper stages or satellites are composed of metallic structures, this phenomenon is anticipated to occur in low Earth

* https://www.kenkai.jaxa.jp/eng/crd2/index.html

orbit (LEO) due to the influence of the geomagnetic field. Assuming the rocket body rotates as a rigid body, the equation governing the attitude motion can be formulated as follows:[13, 14]

$$\mathrm{I}\dot{\boldsymbol{\omega}} + \boldsymbol{\omega} \times (\mathrm{I}\boldsymbol{\omega}) = \boldsymbol{\tau}_{GG} + \boldsymbol{\tau}_{EC} \tag{1}$$

where I is the inertia matrix of the rocket body, and $\boldsymbol{\omega}$ is the angular velocity vector to the inertial system. The gravity gradient torque, $\boldsymbol{\tau}_{GG}$, is

$$\boldsymbol{\tau}_{GG} = \frac{3\mu_G}{R_0^3}\left[\frac{\boldsymbol{R_0}}{R_0} \times \left(\mathrm{I} \cdot \frac{\boldsymbol{R_0}}{R_0}\right)\right] \tag{2}$$

where μ_G is the gravity constant, and $\boldsymbol{R_0}$ is the position vector from the center of the Earth.

The net torque generated by the eddy currents, $\boldsymbol{\tau}_{\mathrm{EC}}$, can be expressed as followings:

$$\boldsymbol{\tau}_{EC} = -\boldsymbol{B} \times S(\boldsymbol{\omega} \times \boldsymbol{B}) \tag{3}$$

where $\boldsymbol{B}$ is the Earth's magnetic field vector, and S is the magnetic tensor. To simplify the simulation, the Earth's magnetic field is assumed to be a simple dipole and that can be calculated as

$$\boldsymbol{B} = \frac{\mu_0 \mu_E}{4\pi R_0^3}\left[\frac{3(\boldsymbol{k}_E^T \boldsymbol{R}_0)\,\boldsymbol{R}_0}{R_0^2} - \boldsymbol{k}_E\right] \tag{4}$$

where $\mu_0 = 1.257 \times 10^{-6}$ NA^{-2} is the magnetic constant, $\mu_E = 7.94 \times 10^{22}$ Am^2 is the Earth's magnetic dipole moment, and $\boldsymbol{k}_E$ is the dipole unit vector, which is inclined about 11.5° to the Earth's rotation axis.

The magnetic tensor S in Eq. (3) is difficult to determine with high accuracy. This simulation was based on a simple cylindrical model with hemispherical caps, using parameters derived from the dimensions and material thickness of the propellant tank.[15] To explore the sensitivity of the simulation results to the magnetic tensor, two different configurations, denoted as Case 1 and Case 2, are considered. The magnetic tensor of Case 1 was computed using the exact tank diameter and thickness along with the total rocket body length. The magnetic tensor of Case 2 was calculated using only the exact diameter, thickness, and length of the fuel tank, excluding contributions from other metallic components such as the oxidizer tank or engine nozzle. Table 1 presents the inertia matrix and the magnetic tensors used in this simulation. The initial condition of the attitude motion is assumed to exhibit a body-axis rotation of 1 deg/sec. The altitude and the inclination are representative for the general LEO rocket body, which was in a sun synchronous orbit at launch.

Table 1 Inertia and magnetic tensor

Inertia Matrix	diag(27.0, 27.0, 6.5) x 10^3 (kg m^2)
Magnetic tensor (case 1)	diag(8.04, 8.04, 8.50) x 10^6 (S m^4)
Magnetic tensor (case 2)	diag(2.76, 2.76, 4.41) x 10^6 (S m^4)
Altitude	600 (km)
Inclination	98°
initial angular velocity in Body frame [x, y, z]	[0, 0, 1]°/s

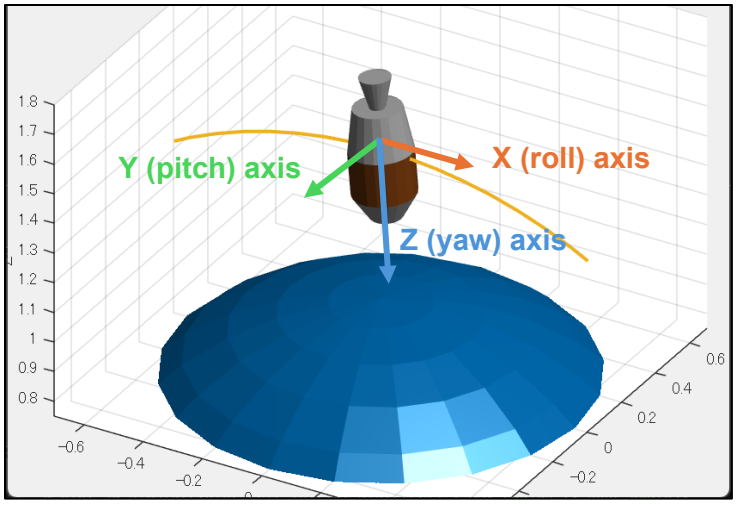

Figure 1. Simulation Coordinates definition (LVLH coordinates axes)

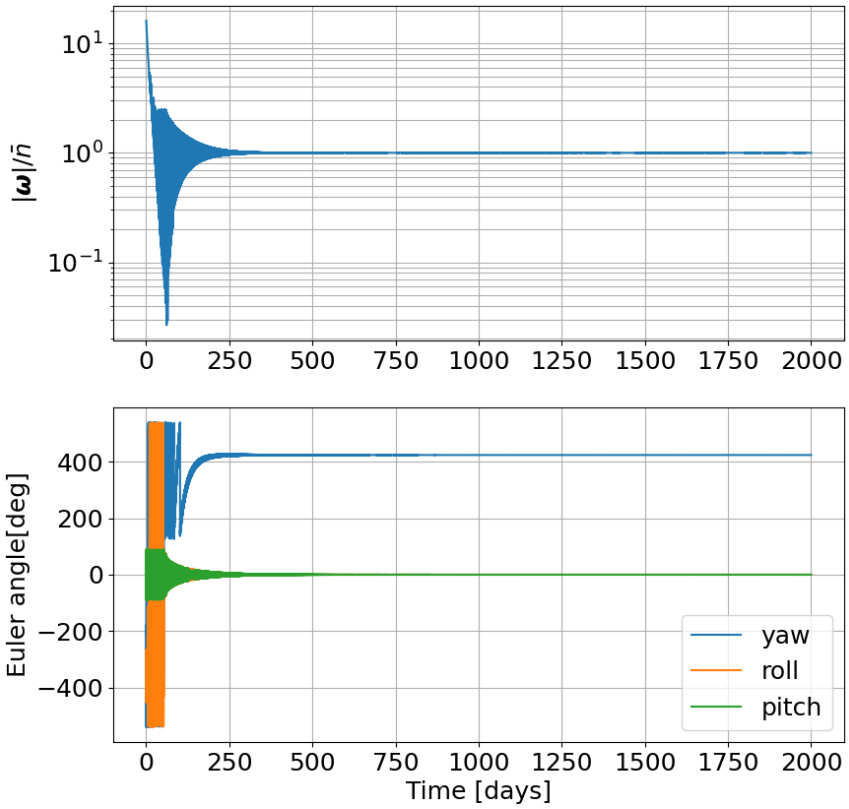

Figure 2. Temporal evolution of angular velocity and attitude Euler angle for Case 1

Top: Angular velocity norm evolution normalized by the orbital mean motion $\bar{\boldsymbol{n}}$
Bottom: Attitude Euler angles (321 convention relative to the LVLH frame) evolution

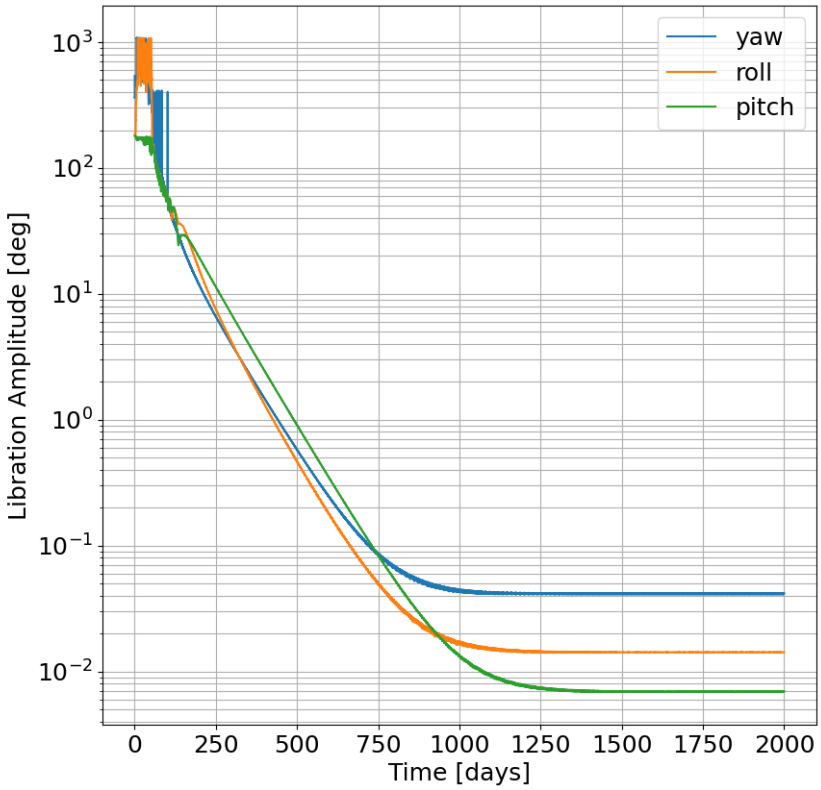

Figure 3. Amplitude of attitude libration angle (321 convention) evolution

The simulation coordinate system is illustrated in Figure 1. Figure 2 and 3 show the results obtained using Eq. (1). The temporal evolution of the simulated angular velocity and attitude angles can be seen in Figure 2, providing insights into the stabilization process. Initially, the rocket body rotates along its body axis, as defined by the initial conditions.

In the top panel of Figure 2, the normalized angular velocity norm shows an initial rapid decrease, eventually stabilizing near a value of one after approximately 300 days. In this context, a normalized angular velocity of one indicates that the angular velocity matches the mean orbital motion, signifying a gravity-gradient-stabilized Local Vertical Local Horizontal (LVLH) attitude. The eddy current torque gradually reduces the angular velocity, leading to tumbling. Once the angular velocity falls below the orbital motion rate, the rocket body begins libration within the LVLH frame due to the dominance of the gravity-gradient torque over the eddy current torque. After 300 days, the attitude motion stabilizes within the LVLH frame.

Figure 3 illustrates the progression of the libration angles, which converge after about 1,000 days. The libration angles were calculated as the maximum deviations from the 110-days average of the respective Euler angle. The pitch and roll librations exhibit amplitudes on the order of 0.01°, while the yaw libration reaches an amplitude of approximately 0.04°. This behavior is explained by the interplay between orbital motion and eddy current torque. A balance angle emerges where the gravity-gradient torque and the eddy current torque resulting from orbital

motion reach equilibrium. As a result, the rocket body exhibits small-angle librations centered around this balance angle.

Figure 4 illustrates the results for the second magnetic tensor configuration (Case 2), revealing stabilizing behavior that is generally consistent with that of Case 1. However, in Case 2, the attitude motion stabilizes within the LVLH frame after approximately 1,000 days, longer than in Case 1. As expected, these findings indicate that the magnetic tensor significantly influences the time needed to stabilize the attitude motion. Although the initial rotational velocity somewhat influences this, its impact is relatively minor, and the overall stabilization behavior aligns closely with the trends observed in Figure 3 and 4.

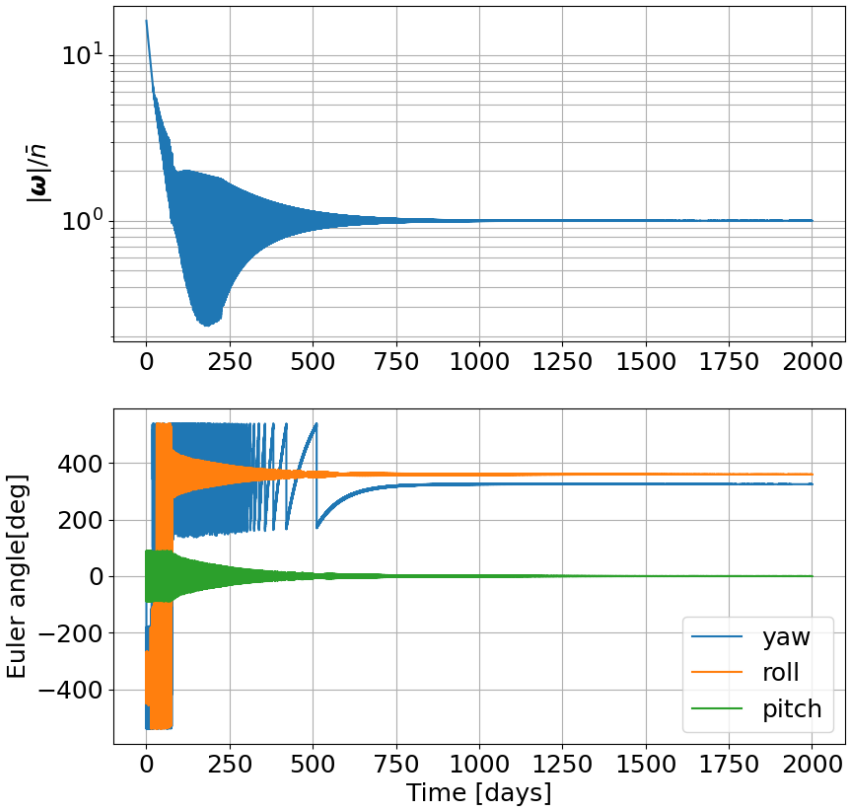

Figure 4. Temporal evolution of angular velocity and attitude Euler angle for Case 2

Top: Angular velocity norm evolution normalized by the orbital mean motion $\bar{\boldsymbol{n}}$
Bottom: Attitude Euler angles (321 convention relative to the LVLH frame) evolution

The exact orbit of the H-II A upper stage has small but non-negligible eccentricity, and the effect of this eccentricity is studied in the following. Using Eq. (1), the temporal evolution of the attitude motion can be simulated under the following assumptions:

- The orbit is near-circular, with a small but non-negligible eccentricity. The orbital elements used in this simulation is shown in Table 2.
- The nodal regression and the apsidal rotation rates are constant as

$$N = -\frac{3}{2} J_2 \frac{R_E^2}{p^2} \bar{n} \cos i$$
$$A = \frac{3}{4} J_2 \frac{{R_E}^2}{p^2} \bar{n}(4 - 5\sin^2 i) \quad (5)$$

where N is the nodal regression rate, A is the apsidal rotation rate, $p = a(1 - e^2)$, a is the semi-major axis, e is the eccentricity, R_E is Earth's equatorial radius, $\bar{n}$ is the mean motion (including J_2 effect), and J_2 = 1.0826 x 10^{-3}, the second zonal harmonic of the geo potential.

The initial conditions for the attitude motion are identical to the zero-eccentricity case, with an initial body-axis rotation of 1°/sec. Figure 5 depicts the evolution of the angular velocity norm, Euler angles, and libration angles over 2,000 days. The top panel of Figure 5 indicates that the debris' attitude motion gradually decreases and stabilizes within the LVLH orientation over several years, similar to the zero-eccentricity case. However, in Figure 5, the bottom panel shows that the amplitude of attitude libration differs from the zero-eccentricity scenario.

The simulation revealed that pitch and roll libration stabilized at approximately 1° after 750 days, while the yaw libration amplitude reached approximately 800° under the given parameters. From this figure, the yaw libration period is calculated to be 110 days, which closely aligns with the apsidal rotation rate influenced by the J2 effect in Eq. (5). This suggests a potential relationship between yaw libration and apsidal rotation. A future, more detailed investigation is necessary to understand this motion fully.

The calculated periods of pitch and roll libration appear similar to the orbital motion period, indicating a possible connection to orbital eccentricity. Figure 6 illustrates the roll and pitch libration angles after 1,500 days, showing convergence to approximately 1°. The libration amplitude fluctuates with a periodicity of about 10 days. A reciprocal relationship is observed, where a decrease in pitch libration amplitude corresponds to an increase in roll libration amplitude, and vice versa. This phenomenon also requires further investigation for a comprehensive understanding.

Overall, the rocket body's attitude motion is expected to stabilize in the LVLH frame while maintaining small librations across all axes.

Table 2 Orbital elements and simulation condition

Altitude	600 km
Eccentricity	0.005
Inclination	98°
Argument of perigee (initial)	0°
Right ascension of the ascending node (initial)	0°
initial angular velocity in Body frame [x, y, z]	[0, 0, 1] (°/s)

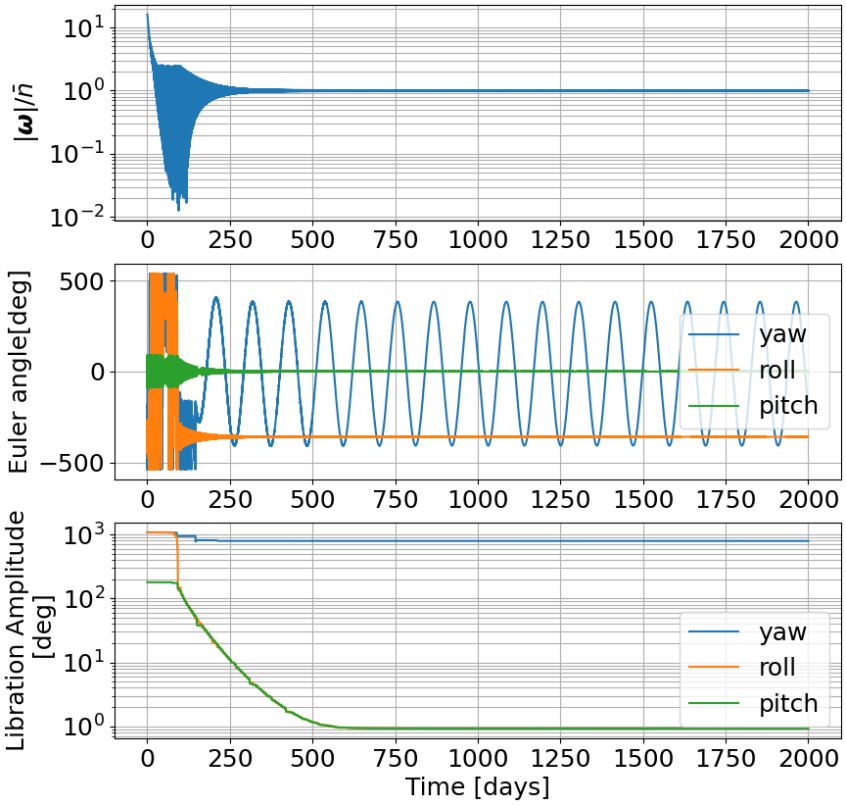

Figure 5. Angular velocity norm, Euler angles, and amplitudes of libration (small eccentricity orbit)

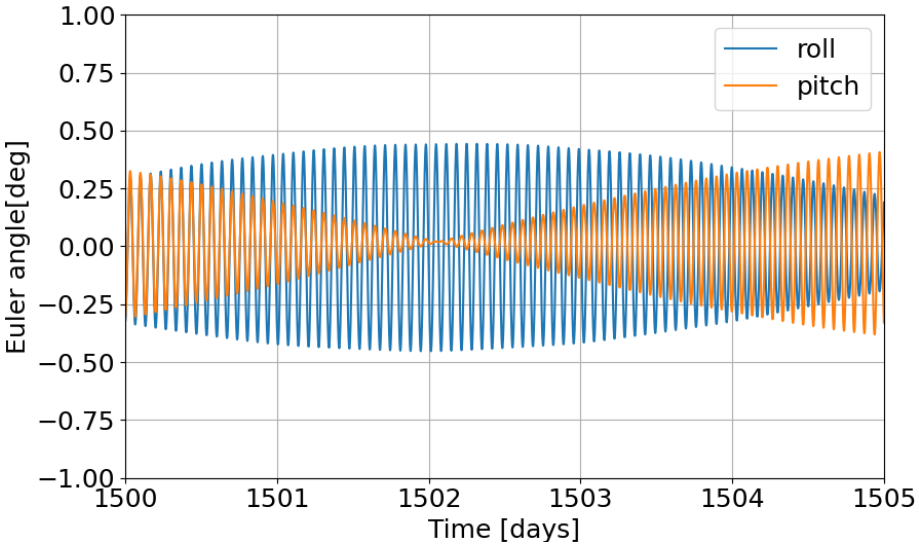

Figure 6.Amplitude of attitude libration (small eccentricity orbit, enlarged)

OBSERVATION FROM THE GROUND

In order to monitor the attitudes of a selected number of spent H-IIA rocket upper stages, JAXA assigned a long-term observation campaign with the Tracking and Imaging Radar system (TIRA)[9, 10], operated by Fraunhofer FHR, Germany. TIRA exhibits two integrated pulsed radars, the narrow band tracking radar at L-band and the broad band imaging radar at Ku-band. The data acquired with both radars were used to analyze the status of the upper stages. The imaging data was processed by means of the Inverse Synthetic Aperture Radar (ISAR) principle. The ISAR images were further analyzed by 3D modelling[11] to estimate the attitudes, rotational velocities and intactness of the selected targets. The 3D geometrical dimensions and shape of the upper stages were provided by JAXA.

Slant range and cross range span the image plane of ISAR images. Slant range information along the line of sight is obtained through the time delay between transmitting a radar pulse and receiving its echo reflected by the target. Cross range is perpendicular to slant range and can be estimated by exploiting the relative rotation between the radar sensor and the object. This relative rotation can be expressed by a rotation vector $\vec{\Omega}$. It is composed of an apparent rotation induced by the object's translational motion along its orbit and the Earth's rotation, but can additionally contain a superimposed intrinsic rotation of the observed object $\vec{\omega}$.

The cross-range-scaling depends on the modulus of $\vec{\Omega}$ that is perpendicular to the line of sight (slant range). In order to compute properly scaled ISAR images, $\vec{\Omega}$ and thus $\vec{\omega}$ has to be known a priori. This is usually not the case. Consequently, ISAR images were processed with a first-guess rotation vector, for example, assuming no intrinsic rotation in Earth-centered inertial (ECI) coordinates ($\|\vec{\omega}\| = 0$ °/s) or a gravity-gradient attitude rotation ($\|\vec{\omega}\| \approx 0.062$ °/s for the upper stage in Figure 3). If the first-guess rotation vector does not fit the data, $\vec{\omega}$ has to be estimated. In order to solve this problem, a 3D model of the object is manually adapted to a series of ISAR images of one observation such that its 2D projection matches the incorrect cross-range-scaled images. This is done by assigning distinct model points to corresponding points in a series of ISAR images. Consequently, a rotation vector $\vec{\omega}$ can be estimated that fits the sequence of assigned model positions best under the assumption that $\vec{\omega}$ is constant over the duration of the pass in ECI coordinates.

The model-based approach for estimating $\vec{\omega}$ requires two conditions to be fulfilled. First, dedicated points on the target have to be unambiguously identifiable in a series of ISAR images. Second, scattering centers—the bright spots in the ISAR images—are assumed to be stationary localized on the target, i.e. they do not move with respect to the object. Both conditions are not or only partially fulfilled in the case of rocket upper stages. These targets are approximately rotational symmetric about their long axis which does not allow to unambiguously identify certain points over a series of ISAR images. Furthermore, because of the large proportion of cylindrical surfaces, many scattering centers in the ISAR images move relative to the target during a series of ISAR images. Thus, the analyst has to induce an unknown rotation about the symmetry axis to assign the 3D model properly. It turned out that the estimated rotational velocities of a slow rotating (< 0.2 °/s) and unstable upper stage had an error of more than 40 % in this campaign. Thus, its estimated $\vec{\omega}$ had no useful meaning. However, if it is likely that an upper stage is stable in a fixed attitude and does not significantly rotate about its symmetry axis, this a priori information can be used to verify the assumed attitude of the observed target with high confidence.

Table 3 Selected TIRA radar observations

#	Date	Acquis. time [UTC]	CPA* range	Max. elevation
1	12 Nov. 2021	11:42:26 – 11:52:18	641 km	84.2°
2	21 Feb. 2022	12:10:03 - 12:19:03	684 km	64.3°
3	23 Mar. 2022	12:01:10 – 12:09:17	643 km	86.6°
4	13 Feb. 2023	12:45:53 – 12:53:50	647 km	80.0°
5	17 Nov. 2023	13:44:04 – 13:52:03	570 km	88.4°
6	19 Feb. 2024	14:01:47 – 14:11:01	571 km	85.1°

* CPA: Closest Point of Approach to the radar sensor

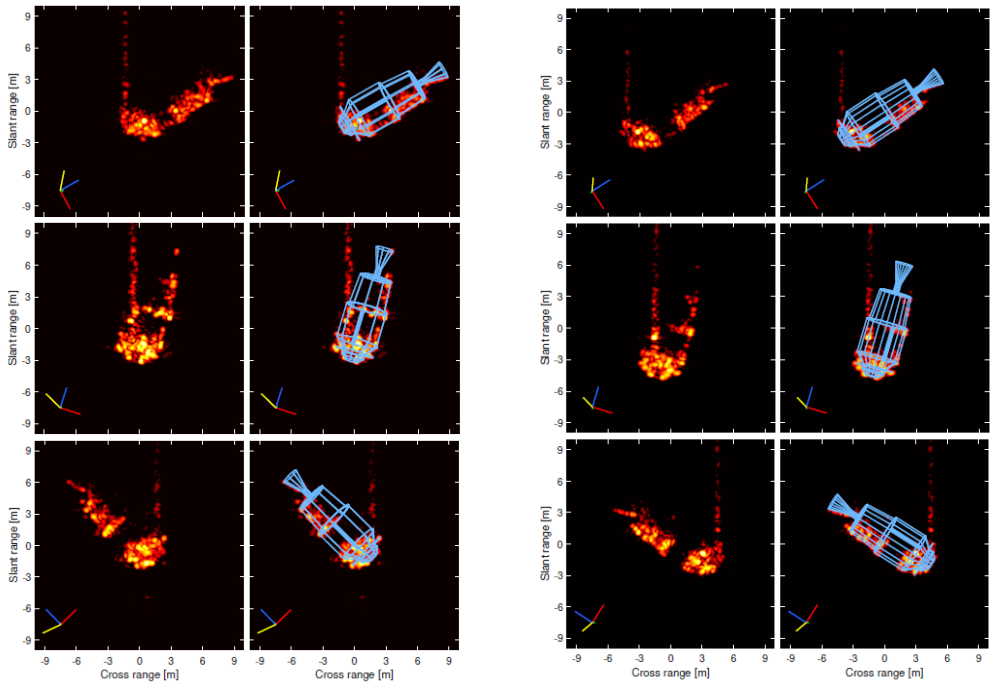

Figure 7 ISAR images of H-IIA rocket body.

Left: Observed on November 21, 2021, Max elevation: 84.2°.
Right: Observed on February 24, 2024, Max elevation: 85.1°.

The upper stage presented here showed a stable attitude over a period of several years. Table 2 provides a summary of selected TIRA radar observations conducted to date, while Figure 3 presents the ISAR images alongside the 3D model matching results from observations #1 and #6, respectively. The upper stage shown in Figure 3 is pointing towards nadir with its nose oriented towards the Earth. This is apparent by comparing the upper stage's attitude with the blue vector in the lower left corner of the ISAR images. The blue vector represents the radial vector of the orbit. Range extended returns (RERs) originate from the rocket's nose visible as vertical scattering center patterns in positive slant range direction. RERs are the result of multiple reflections of radar pulses at the target before backscattering to the sensor. Multiple reflections increase the roundtrip time and are detected as increased range, since slant range information is obtained through the time delay between transmitting a radar pulse and receiving its echo. Here, the radar pulses were reflected multiple times within a cavity located at the nose of the H-IIA upper stage. In order to image the maximum extent of the target, passes with high elevations at the closest point of approach (CPA) were observed. Not only its shape is clearly visible and matches the model appropriately, but also sidewards extending parts of the Payload Attachment Fitting (PAF) could be identified during all observed passes. This reduced the degree of rotational symmetry and thus allowed to exclude a significant rotation about the long axis.

ON ORBIT OBSERVATION RESULT

ADRAS-J was launched on 18. Feb. 2024 by Electron rocket of Rocket Lab from Launch Complex 1, New Zealand. After orbital insertion, ADRAS-J rendezvoused to the H-IIA upper stage using several navigation's means, i.e. GPS absolute navigation, Angles Only Navigation (AON), and Model Matching Navigation (MMN). Finally, ADRAS-J was approaching the H-IIA upper stage within 50 m distance and obtaining optical images.

A fixed-point observation, during which the relative position remained stable for one full orbit, was conducted from approximately 50 meters behind the H-IIA upper stage. Figure 8 provides a representative example of an image captured during this observation. In the figure, the relative position is depicted using the RIC coordinate system, where R is positive upward, C is positive to the left, and I is normal to the page, pointing away from the reader. The origin of the coordinates is assumed to be at the H-IIA upper stage's center of mass.

The H-IIA upper stage remained nearly stationary in a gravity-gradient stabilized attitude, with the Payload Attachment Fitting (PAF) side oriented toward the Earth's center, aligning the main axis of the rocket body with the direction of gravity. According to the numerical simulation as discussed in the previous section, when an object is in an orbit with a relatively small eccentricity within the gravity-gradient stable range, eddy current torques generated by interactions with the geomagnetic field can dampen its attitude motion, leading to a gravity-gradient stabilized state. This observation has confirmed the existence of such a condition in practice.

The attitude motion of the H-IIA upper stage remained in a gravity-gradient stabilized state throughout one orbital period of the fixed-point observation, with a minimal inclination of its principal axis. During this period, the client appeared nearly stationary. The straight section of the target was measured in the image and found to be inclined by approximately 0.97° to LVLH frame.

Following the fixed-point observation, a fly-around maneuver was executed to obtain images of the H-IIA upper stage from various perspectives, providing a more comprehensive assessment of its attitude. ADRAS-J conducted a fly-around observation maintaining a relative distance of 50 meters while circumnavigating the H-IIA upper stage in approximately 40 minutes. Figure 9

presents three images captured during both the fixed-point and the fly-around observations, with ADRAS-J positioned near the v-bar of the LVLH frame.

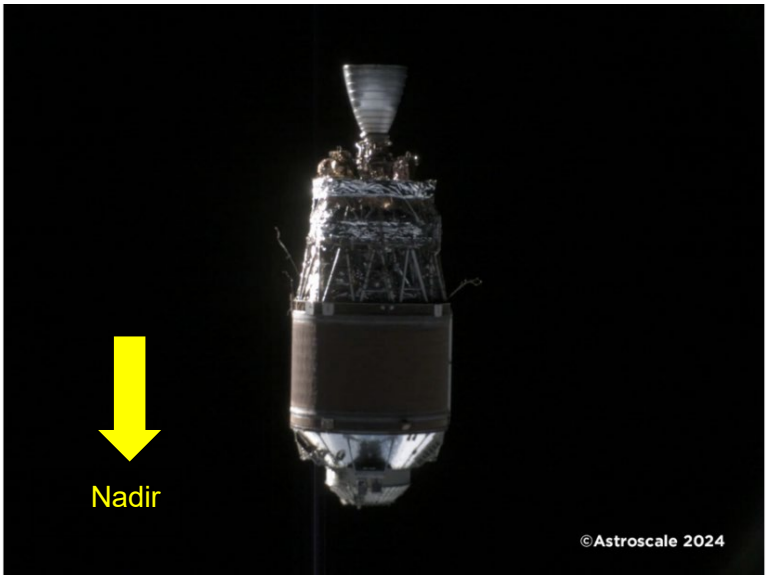

Figure 8 Fixed Point Observation Image

Image captured on 2024/5/23 4:32:52 at distance of R= 0.35 m, I= -49.3 m, and C= -0.28 m. ADRAS-J attitude to LVLH is roll= -0.00933°, pitch= -0.624°, and yaw= 0.416°.

From the captured images, the inclination of the rocket body relative to the image frame was determined. The measurement was conducted using the straight section of the rocket body, with an accuracy of ±0.4° due to pixel-related errors. By incorporating the ADRAS-J's attitude data, the roll attitude of the H-IIA upper stage was estimated and is summarized in Table 4. As seen from Table 4, the measured roll angles fall within a range of approximately ±1°, closely corresponding to the results predicted by the numerical simulations of the previous section.

During the ADRAS-J operation, the H-IIA rocket body has been in gravity gradient stable attitude as predicted by the numerical simulation and FHR TIRA observation results. Further investigations will be required to comprehensively explain this attitude motion.

Table 4 Estimated H-IIA roll attitude to LVLH

#	Date	Acquis. time [UTC]	Estimated roll angle relative to LVLH [°] (accuracy ±0.4°)
1	2024/5/23	4:32:52	0.97°
2	2024/7/15	7:17:08	-1.19°
3	2024/7/15	7:41:32	0.14°

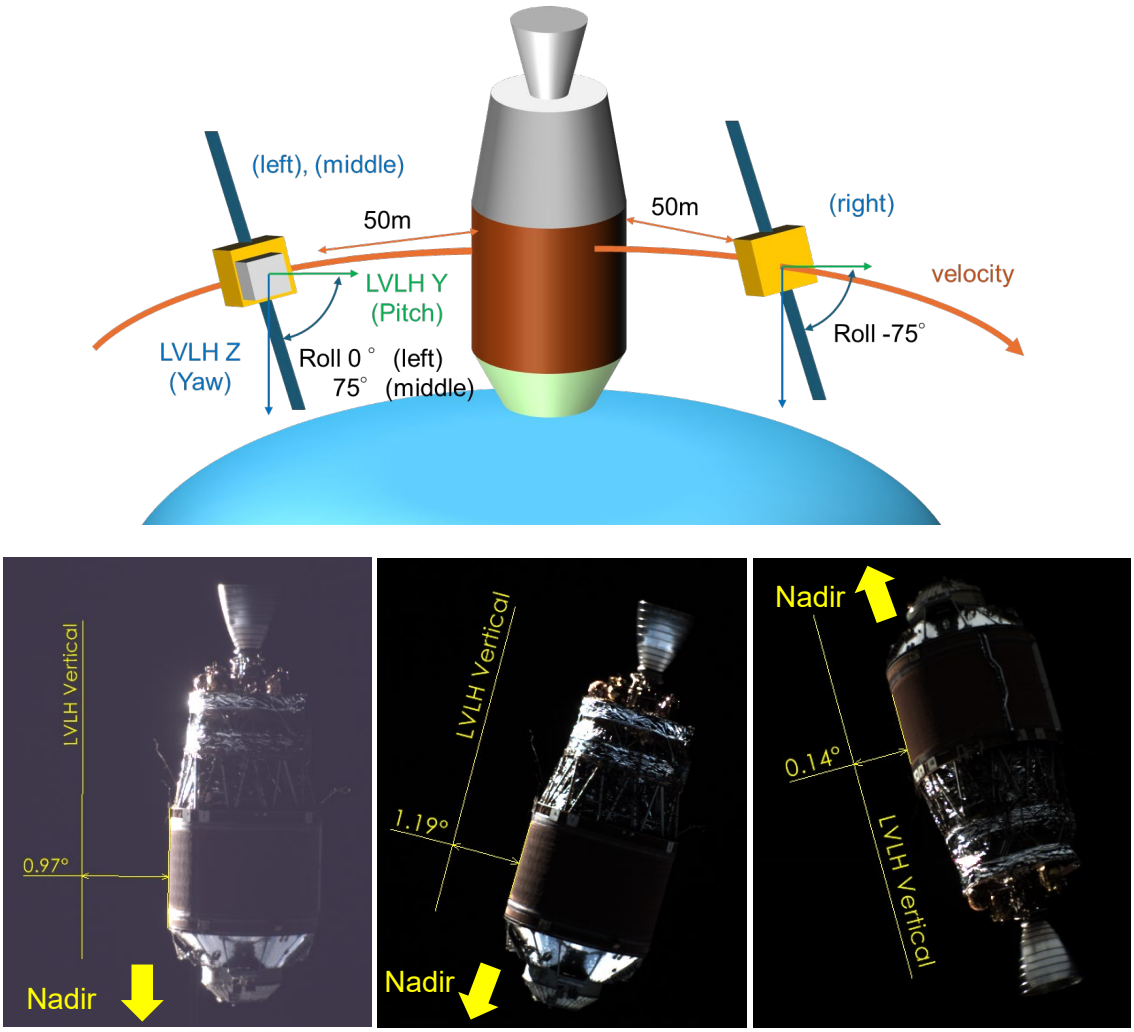

Figure 9 Rocket body inclination in each image

Top: Illustration depicting ADRAS-J's position and attitude relative to the target.
Bottom: Images captured by ADRAS-J under the following attitude conditions:
Left: 2024/5/23 4:32:52 ADRAS-J's attitude to LVLH (R, P, Y) = (-0.009°, -0.624°, 0.416°)
Middle: 2024/7/15 7:17:08 ADRAS-J's attitude to LVLH (R, P, Y) = (75.0°, -0.096°, -0.038°)
Right: 2024/7/15 7:41:32 ADRAS-J's attitude to LVLH (R, P, Y) = (-74.6°, -14.0°, 176.0°)

CONCLUSION

This research contributes to a growing body of knowledge that is essential for mitigating the risks posed by space debris and ensuring the long-term sustainability of space activities.

The numerical simulations, incorporating both gravity-gradient torque and eddy current torque induced by the geomagnetic field, predicted that the long-term orbiting rocket upper stage would gradually obtain a gravity-gradient-stabilized attitude. Ground-based observations of the object

obtained with the TIRA system of Fraunhofer FHR over a three-year period between November 2021 and February 2024 confirmed that the H-IIA upper stage had evolved into such a stable state. Subsequently ADRAS-J approached this rocket upper stage in May 2024, and continuous optical observations from a 50-meter distance verified that it maintained an approximately LVLH-aligned attitude. These findings provide valuable insights for the development of capture mechanisms and control algorithms for future ADR missions targeting similar debris objects. For example, as the H-IIA upper stage is projected to maintain a gravity-stabilized attitude, the ADR mission's rendezvous trajectory planning for this target can rely on the assumption that its attitude motion is relatively stable and predictable. Moreover, estimating the time required for the capture sequence has become feasible, which is a critical factor in the overall design of the ADR spacecraft system.

Ground-based radar observations generally confirmed the stabilized attitude, while on-orbit optical imagery additionally revealed a slight and slow libration in the object's motion behavior. The nearly circular orbit facilitates the reduction of angular momentum through eddy current torque, allowing stabilization near the LVLH frame. However, orbital eccentricity introduces slight librational motion into the attitude dynamics.

Over the course of several months, ADRAS-J captured an extensive series of images. Future research will focus on refining the numerical model to incorporate a more comprehensive representation of the geomagnetic field and the material properties of the debris. In addition, a detailed analysis of the full dataset of ADRAS-J imagery will allow to further characterize the libration dynamics and validate the numerical predictions.

REFERENCES

[1] J.-C. Liou, "An active debris removal parametric study for LEO environment remediation," Advances in Space Research, 47, pp. 1865–1876, 2011

[2]] Minghe Shan, Jian Guo, Eberhard Gill, "Review and comparison of active space debris capturing and removal methods," Prog. Aerosp. Sci. 80, pp. 18–32 January 2016.

[3] Silha J, Pittet JN, Hamara M, and Schildknecht T, "Apparent rotation properties of space debris extracted from photometric measurements," Advances in Space Research, 61, pp. 844-861, 2018

[4] Alessandro Vananti; et al., "Attitude Estimation of H2A Rocket Body from Light Curve Measurements," Int. J. Astrophys. Space Sci. 2023, 11(2), 15-22. https://doi.org/10.11648/j.ijass.20231102.11

[5] Schildknecht, T., et al., "Determining, Monitoring and Modelling the Attitude Motion of Potential ADR Targets," Clean Space, Industrial Days, May 2016.

[6] Kozhukhov, O. M., et al. "Photometric patterns as a key for determining the orientation of the rotation axis of RSO." Advanced Maui Optical and Space Surveillance (AMOS) Technologies Conference, 2024.

[7] Yamamoto, Toru, et al. "Pave the way for active debris removal realization: Jaxa commercial removal of debris demonstration (CRD2)," 8th European Conference on Space Debris, 2021.

[8] Nakamura, Ryo, et al., "Study on Technology Demonstration Scenarios of CRD2 Phase2 for Sustainable Debris Removal," 2nd International Orbital Debris Conference (IOC II), 2023.

[9] D. Mehrholz, "Space object observation with radar," Advances in Space Research, Volume 13, Issue 8, pp. 33-42, ISSN 0273-1177, 1993, https://doi.org/10.1016/0273-1177(93)90565-S.

[10] J. Klare and et, al., "The Future of Radar Space Observation in Europe—Major Upgrade of the Tracking and Imaging Radar (TIRA)," Remote Sens. 2024, 16, 4197. https://doi.org/10.3390/rs16224197

[11] S. Sommer, J. Rosebrock, D. Cerutti-Maori, and L. Leushacke, "Temporal analysis of Envisat's rotational motion," JBIS, February – April 2017, Volume 70, pp. 45-51.

[12] Eijiro Atarashi, et al., "ULTRA-CLOSE RPO ON-ORBIT DEMONSTRATION OF ADRAS-J PROGRAM," 22nd IAA Symposium on Space Debris, 2024.

[13] Mitani, Shinji, et.al. "Dynamical Feature Estimation of an On-orbit Debris Using Only Gyroscope Information", Proceedings of the 65th Space Sciences and Technology Conference, 1A10, 2021. (In Japanese)

[14] Efimov, S., Pritykin, D., and Sidorenko, V., "Long-term attitude dynamics of space debris in Sun-synchronous orbits: Cassini cycles and chaotic stabilization", *Celestial Mechanics and Dynamical Astronomy*, vol. 130, no. 10, Art. no. 62, Springer, 2018. doi:10.1007/s10569-018-9854-4.

[15] N. Gomez et. al.: "Eddy Currents applied to Detumbling of Space Debris: Analysis and Validation of Approximate Proposed Methods," Acta Astronautica, 2015.